

# SERS studies of explosive molecules with diverse copper nanostructures fabricated using ultrafast laser ablation

Hamad Syed<sup>1,2</sup>, G. Krishna Podagatlapalli<sup>2</sup>, M. A. Mohiddon<sup>3</sup>, Venugopal Rao Soma<sup>2\*</sup>

<sup>1</sup>School of Physics, University of Hyderabad, Prof. C.R. Rao Road, Gachibowli, Hyderabad 500046, India

<sup>2</sup>Advanced Center of Research in High Energy Materials (ACRHEM), University of Hyderabad, Prof. C.R. Rao Road, Gachibowli, Hyderabad 500046, India

<sup>3</sup>National Institute of Technology Andhra Pradesh, Tadepalligudem, Andhra Pradesh 534101, India

\*Corresponding author. Tel: (+91) 040-23138811; E-mail: soma\_venu@uohyd.ac.in

Received: 13 June 2015, Revised: 25 October 2015 and Accepted: 04 November 2015

## ABSTRACT

We report the fabrication and application of ultra-short pulse laser induced nanostructures (NSs) on copper surface accomplished with different pulse energies and number of pulses. The shapes and sizes of NSs have been evaluated from the field emission scanning electron microscopy (FESEM) data which illustrated different ablation mechanisms in picosecond (ps) and femtosecond (fs) domains. The Cu NSs generated with ps pulses demonstrated Raman enhancements upto  $\sim 10^5$ - $10^8$  in the case of the explosive molecules of 1,1-diamino-2,2-dinitroethene (FOX-7), 5 Amino, 3-nitro,1,3,5-nitroazole (ANTA) and 2,4,6,8,10,12-Hexanitro-2,4,6,8,10,12-hexaazaisowurtzitane (CL-20). The SERS studies were repeated two more times on the same substrate following a simple cleaning procedure. We achieved considerable enhancement factors (of  $>10^5$ ) for the Raman modes of an explosive molecule of FOX-7 on fs laser fabricated Cu NSs. Copyright © 2015 VBRI Press.

**Keywords:** Laser ablation; picosecond; femtosecond; explosives detection; SERS.

## Introduction

The inherent weak Raman scattering cross-section of any molecule can be comprehensively enhanced by introducing surface effects resulting from plasmonic nanomaterials (NMs) placed in their vicinity. This effect is called as surface enhanced Raman scattering (SERS) [1-5]. SERS has been proved to be one of the most proficient techniques for detection of trace level organic [6], biological [7, 8], explosive molecules such as RDX (1, 3, 6-trinitroperhydro-1, 3, 5-triazine) and TNT (trinitrotoluene) [6, 7-13], Rhodamine 6G, crystal violet, and bacteria etc. Detection of explosive molecules in trace amounts is a challenging task in present times with no single technique capable of unambiguous and rapid detection. Fox-7 a derivative of DADNE (1,1-diamino-2,2-dinitroethene; a high explosive), ANTA (5-amino-3-nitro-1,2,4-triazole, an insensitive high explosive), and CL-20 (2,4,6,8,10,12-Hexanitro-2,4,6,8,10,12-hexaazaisowurtzitane; a nitramine explosive) are some of the explosive molecules with potential use in propellant and military applications. It is important to contrive techniques which can rapidly detect such molecules (and similar ones) and in very low concentrations (nanomolar or even lower). Over the last few years SERS has been successfully utilized to detect even attomolar concentration of analyte molecules

(including a few explosive molecules) with fairly high reproducibility. This was possible with development of novel SERS substrates using a variety of physical and chemical methods. However, there are several main challenges that need to be addressed before this technique is used for routine analysis like other spectroscopic techniques. Specifically the scientific community should address the challenges of (a) preparation of large area substrates using low-cost procedures (b) uniformity and reproducibility of the nanostructures resulting in uniform enhancements (c) recyclable nanostructures for number of analyte detection (d) demonstrate large enhancements for most of the analyte molecules on single substrate etc. Though this technique is not capable of stand-off detection, it is advantageous for the samples with extremely low concentration can be analyzed rapidly. Such techniques find applications where sufficient time is available for analysis of the samples of interest.

Plasmonic metals such as Ag, Au and Cu in the form of colloids, dried colloids on plain substrates and nanostructures have been utilized for SERS measurements since they can support different types of surface plasmons [14-17]. For example, Mishra *et al.* [15] studied Au as plasmonic metal along with ZnO and achieved significant enhancement in the Raman signal for C<sub>70</sub> molecules.

Mishra *et al.* [17] again used silver nanocup-type structures for SERS studies of  $C_{70}$  molecules. In SERS, any analyte molecule in the neighborhood of NMs experiences the enhanced local field through the excitation of surface plasmons resulting in a large Raman scattering signal from the molecule. This is termed as electromagnetic enhancement and the enhancement factor is dependent on fourth power of local electromagnetic field [18] produced by oscillations of electric dipole at resonance condition. The enhancement is mediated through complex dielectric function with negative real part (provides induced polarization under the effect of incident electromagnetic field) and very less but significant positive imaginary part (provides the absorption of the light by material). Different plasmonic material nanoparticles (NPs) architectures, roughened nanostructures (NSs), laser induced periodic surface structures (LIPSS) have been demonstrated to contribute towards Raman enhancements [6, 11-13].

Ultrafast laser ablation in liquid media (ULAL) is a unique processing technique to efficiently fabricate the plasmonic NMs [19-22] supporting localized surface plasmons (LSPs), propagating surface plasmons or both. Yang's group [23-25] had pioneered the technique of nanosecond laser ablation in liquids. Some of the previous works [26-32] projected a few feasible mechanisms for the fabrication of random NSs and LIPSS (with period of nearly half the laser wavelength) in metals achieved through ps/fs laser ablation. Skolski *et al.* [33] reported the experimental and theoretical investigation on the formation of high/low spatial frequency LIPSS (HSFL/LSFL) on metals using ultrafast lasers. Huang *et al.* [34] investigated the mechanisms on the formation of sub-wavelength nanoripples on solid surfaces and demonstrated that target surface ablated by ultrashort laser pulses at damage threshold fluence should act as metal. Derrien *et al.* [35] explored the mechanisms of ripple formation on Si achieved using fs pulses and evaluated the role of excited free carriers density. Recently, our group [36] had observed that complex refractive index and conduction band electron density played a crucial role in determining the periodicity of HSFL. Several authors [30, 37] have investigated the intrinsic mechanisms of laser induced periodic surface nanostructure formation in Au, Ag and Cu, demonstrating that the Cu is a suitable metal permitting the formation of LIPSS compared to Ag and Au. The following reasons could be envisaged for the efficient formation of LIPSS on Cu surface (a) the probability of interference between surface polariton wave ( $k_{sp}$ ) and incident wave ( $k_{in}$ ) is higher for Cu [ $k_{sp}/k_{in} \sim 1$ ] (b) Cu demonstrated a large electron-phonon coupling constant ( $\gamma$ ) value ( $1 \times 10^{17}$ ) in comparison with Ag ( $0.36 \times 10^{17}$ ) and Au ( $0.21 \times 10^{17}$ ) since the electron-phonon sub system is compatible for generating a non-uniform heat or energy distribution spatially, resulting in the production of LIPSS [37]. In previous reports the phenomena were discussed for ablation performed in air/vacuum whereas in the present work we carried out ablation in liquid media. In one of our earlier works [11] we had reported the fabrication of Cu NSs in diverse liquid media using picosecond (ps) pulses and achieved significant Raman enhancements from the substrates thus prepared. The ablation phenomena,

especially in the presence of a liquid medium, is an extremely complicated process depending extensively on various parameters such as (i) input pulse duration (ii) input pulse energy (iii) wavelength of excitation (iv) the number of input pulses (v) surrounding liquid (refractive index, viscosity, etc.) (vi) focusing conditions (Gaussian/Bessel; normal focusing versus cylindrical focusing) (vii) beam quality (Gaussian, top-hat etc.) (viii) static/scanning ablation etc. Some of these parameters have been investigated in our earlier works [6, 12, 13, 19-21]. It is imperative to investigate the effect of all these parameters on the ablation products and their application in SERS studies to arrive at optimized and efficient substrates for trace molecule detection. In the present work we present results from our detailed studies of (a) the effect of input pulse energy on the morphology of Cu targets ablated in acetonitrile (ACN) using picosecond (ps) pulses (b) SERS studies of an explosive molecule FOX-7 using different Cu NSs prepared using ultra short laser pulses (c) re-utilization of substrates to detect different explosive molecules such as ANTA and CL-20 subsequent to the SERS studies performed on ANTA (d) investigation of the influence of number of pulses (incubation effects) on fabrication of Cu NSs in acetone using femtosecond (fs) pulses (e) demonstration of recyclable nature of the Cu NSs prepared by fs pulses through the SERS studies of FOX-7 and Rhodamine 6G (Rh6G) molecules.

## Experimental

The ps/fs ablation studies were performed using a 1 kHz chirped pulse amplified Ti: sapphire laser system (Coherent) delivering nearly bandwidth limited laser pulses ( $\sim 2$  ps/ $\sim 40$  fs) at 800 nm. The amplifier was seeded with  $\sim 15$  fs (typically 50-55 nm FWHM) pulses from an oscillator (MICRA, Coherent, 1 W, 80 MHz, 800 nm). Complete details of the experiments were reported in our earlier articles [6, 38, 39]. The initial laser beam diameter in the ps case was  $\sim 8$  mm and was focused with 25 cm focal length lens on the surface of Cu substrate placed in ACN. Typical pulse energies of 25–400  $\mu$ J were utilized. Input energy was controlled by the combination of Brewster angle polarizer and a half wave plate. The target was placed normal to the laser beam on a three dimensional motorized stage [Nano-direct] with resolution of  $\sim 25$  nm and was controlled by a controller interfaced to a PC. Duration of each scan was fixed to  $\sim 30$  minutes and line to line spacing was  $\sim 50$   $\mu$ m. To avoid ambiguity fabricated Cu substrates in ACN were designated as CuS-25, CuS-50, CuS-100, CuS-200, CuS-300 and CuS-400 for structures created using pulse energies of  $\sim 25$ ,  $\sim 50$ ,  $\sim 100$ ,  $\sim 200$ ,  $\sim 300$  and  $\sim 400$   $\mu$ J, respectively. Additionally, we have investigated the development of laser induced surface nanostructures on the metal target by varying the speeds (400, 300, 200, 100 and 50  $\mu$ m/s) in the fs case. The beam diameter ( $2\omega_0$ ) estimated on the target in acetone was  $\sim 90$   $\mu$ m. The typical level of liquid above the target surface was  $\sim 5$  mm. The laser beam was focused perpendicularly on Cu plate which was immersed in acetone and Cu plate was positioned on a motorized Nano direct X-Y stage, which was operated through a controller (NTS-25). Typical

fluence used was  $\sim 2.5 \text{ J/cm}^2$ . The number of pulses incident on the target was controlled by varying the speeds of X-Y stages and line-line spacing was  $\sim 25 \mu\text{m}$ . The estimated number of pulses per spot in the focal region  $[w(z)/d]$  w.r.t. scanning speeds were  $\sim 253$ ,  $\sim 300$ ,  $\sim 500$ ,  $\sim 1000$  and  $\sim 2000$  (threshold fluences of  $\sim 0.98$ ,  $\sim 0.95$ ,  $\sim 0.89$ ,  $\sim 0.81$  and  $0.74 \text{ J/cm}^2$ ) for the scanning speeds of 400, 300, 200, 100 and  $50 \mu\text{m/s}$ , respectively. The surface morphology of ablated targets was characterized by FESEM. The surface roughness was measured using a surface profilometer.

## Results and discussion

### Effects of pulse energy on Cu NSs in ACN prepared by ps pulses and SERS studies

The surface morphology of Cu substrates was characterized by FESEM [Ultra 55 from Carl ZEISS instrument] technique. **Fig. 1** illustrates the FESEM images of formed surface nanostructures obtained by ps laser ablation of Cu targets with different energies (a) CuS-25 (b) CuS-50 (c) CuS-100 (d) CuS-200 (e) CuS-300 and (f) CuS-400. We observed random structures at lower input energies (25-100  $\mu\text{J}$ ) whereas LIPSS with different periodicity were observed at higher input energies (200-400  $\mu\text{J}$ ) and was confirmed from the FESEM images.

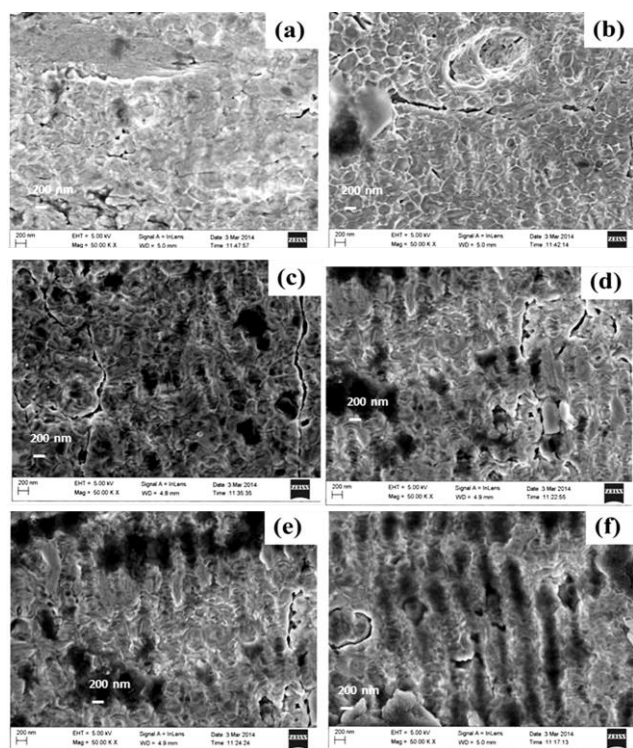


**Fig. 1.** FESEM images of surface nanostructures were fabricated on Cu substrate by ps ablation of bulk Cu in ACN (a) CuS-25 (b) CuS-50 (c) CuS-100 (d) CuS-200 (e) CuS-300 and (f) CuS-400. The scale bar is 200 nm in all the pictures.

To understand and explain the formation of LIPSS on Cu we considered the dynamics in processes of laser interaction with metals which are related to the electron-lattice system. When the ps pulses interact with Cu free

electrons in the metal surface absorb laser pulse energy through inverse Bremsstrahlung and generate surface electromagnetic field. Due to the interaction of incident laser pulse with the generated surface electro-magnetic field, energy can be distributed non-uniformly along the metal surface. This non-uniformly distributed energy can be coupled to electrons and allowed to form electron temperature distribution with a periodic nature. Consequently, the hot electrons couple to lattice and get relax ( $\sim 1 \text{ ps}$ ) while transferring the energy to lattice system. The lattice reorganizes itself at the melting state and is followed by re-solidification. Due to the electron-phonon interactions this ephemeral, two different temperature systems will have a tendency to attain equilibrium temperature within few ps. These electron-phonon interactions can be defined by electron-phonon coupling constant. Therefore, two-temperature model is generally utilized to demonstrate thermal phenomena in the case of ultrafast laser matter attraction. The growth of LIPSS can be demonstrated on the basis of electron-phonon coupling constant ( $\gamma$ ) [37]. It was confirmed that the electron-phonon coupling constant is directly related the electron and lattice temperatures, and these temperatures in turn depend on the fluence incident on the target surface. The input laser fluence should be more than the ablation threshold fluence that could melt the sample surface to generate periodic structures and the earlier reported ablation threshold fluence for Cu was  $1.7 \pm 0.2 \text{ J/cm}^2$  [40]. Following some of the previous reports we understand that the shape of the periodic surface structures change with respect to laser fluence and number of pulses. To explore the fluence effect on the development of the LIPSS on Cu target surface, the evaluation of effective spot size on the Cu target surface for various input laser energies was performed. Laser machined single lines were drawn on Cu target surface and the width of the lines were taken as effective beam diameters of laser beam as suggested by Barcikowski *et al.* [41]. The FESEM characterization validated the differences observed in the estimated spot sizes of  $\sim 65$ ,  $\sim 87$ ,  $\sim 112$ ,  $\sim 130$ ,  $\sim 170$ ,  $\sim 190 \mu\text{m}$  for input energies of  $\sim 25$ ,  $\sim 50$ ,  $\sim 100$ ,  $\sim 200$ ,  $\sim 300$ ,  $\sim 400 \mu\text{J}$ . From the measured spot diameters on the targets, effective number of pulses overlapping within a spot and separation between the lines we could confirm that single line ablation transpired in the case of CuS-25, CuS-50 since the line separation was  $60 \mu\text{m}$  and double line ablation ensued on CuS-100, CuS-200, where the line separation was almost half compared to the spot on target.

We could confirm from our experimental results that periodic patterns were not observed on the Cu surface in the cases of Cu-25, Cu-50 and Cu-100 (**Fig. 1(a-c)**) since the estimated effective input fluences were less than the ablation threshold fluence of  $(1.7 \pm 0.3 \text{ J/cm}^2)$  and the surface r.m.s. roughness (measured separately using a surface profilometer) was found to be  $\sim 0.8 \mu\text{m}$ ,  $\sim 2.7 \mu\text{m}$  and  $\sim 3.6 \mu\text{m}$ , respectively. Comparatively, the periodic pattern, spread over a small area and less evident, in the case of Cu-200 (**Fig. 1(d)**) was formed due to a pulse train of  $\sim 866$  shots at a fluence of  $\sim 3 \text{ J/cm}^2$ . In the cases of Cu-300 and Cu-400 (**Fig. 1(e, f)**), LIPSS on Cu surfaces were expanded and more pronounced at fluences of  $\sim 2.67 \text{ J/cm}^2$  ( $\sim 1700$  shots),  $\sim 2.82 \text{ J/cm}^2$  ( $\sim 1900$  shots), respectively. The

measured periodicity of LIPSS for Cu-200, Cu-300 and Cu-400 were  $\sim 430$  nm,  $\sim 420$  nm and  $\sim 470$  nm, and surface r.m.s. roughness was measured to be  $\sim 2.6$   $\mu\text{m}$ ,  $\sim 2.4$   $\mu\text{m}$  and  $\sim 1.8$   $\mu\text{m}$ , respectively. From the observed data of surface r.m.s. roughness it was concluded that at low input fluence ablation was good and at higher fluences ablation efficiency was decreased. From our knowledge and previous reports we believe that electrons might not transfer the energy to lattice before the expiration of the periodic distribution of electron temperature with a pulse train of fewer shots (input fluence  $\leq$  threshold fluence) due to the active participation of the electron diffusion phenomenon. Therefore, less coupling could have taken place between the electron and lattice, and consequently, resulting in a lower  $\gamma$  value [37]. However, non-uniform surface heat distribution cannot occur at this position which may not produce periodic surface structures on the surface. In the case of more effective number of pulses (input fluence  $>$  threshold fluence), electrons can couple to the neighbour lattice easily to transfer the energy and thermalization will take place between electrons and lattice resulting in a higher  $\gamma$  value ( $\sim 10^{17}$ ) [37]. At this position, lattice will also attain temperature profile with periodic behaviour. Nonetheless, non-uniform heat distribution can occur on the metal surface and, therefore, LIPSS could have formed on the metal surface.

The fabricated structures on Cu substrates fabricated with different pulse energies (25–400  $\mu\text{J}$ ) in ACN were utilized for SERS studies of explosive molecules at low concentrations. **Fig. 2(a)** illustrates the enhanced Raman spectra of FOX-7 molecules [13] which were adsorbed on Cu substrates and they were allowed to dry for  $\sim 1$  hour. All the Raman spectra were recorded using a WITec Alpha 300 spectrometer and an excitation source with a wavelength of 532 nm (cw laser). The sample on the Cu NSs could be recognized through the in-built optical microscope (with an objective lens of 100X) and the spectra were collected by the in-built spectrometer in the WITec instrument simultaneously. The acquisition time used for recording was 5 s and all spectra were calibrated using the Raman peak of Silicon wafer at  $520\text{ cm}^{-1}$ . Typically, a little drop ( $\sim 10$   $\mu\text{l}$ ) of FOX-7 (concentration of 25  $\mu\text{M}$ ) was placed on substrates to achieve a monolayer of the molecules. The Raman spectra revealed that C-NO<sub>2</sub> symmetrical stretch mode corresponding to  $1342\text{ cm}^{-1}$  was predominantly elevated along with other modes. The other observed modes were (a) symmetric NO and NH wagging mode (b) out of layer symmetric NH wagging mode (c) C-NO<sub>2</sub> rocking mode (d) NO and NH rocking mode (e) In-layer asymmetric NH wagging (f) In-layer symmetric NH wagging mode (g) C-C stretch and NH wagging (h) Asymmetric C-NO<sub>2</sub> stretching and NH wagging (i) Out of layer symmetric NH wagging, NO and NH rocking, (j) C-C symmetric +NH stretching modes and (k) NH<sub>2</sub> bending corresponding to  $481\text{ cm}^{-1}$ ,  $620\text{ cm}^{-1}$ ,  $794\text{ cm}^{-1}$ ,  $858\text{ cm}^{-1}$ ,  $1024\text{ cm}^{-1}$ ,  $1065\text{ cm}^{-1}$ ,  $1169\text{ cm}^{-1}$ ,  $1205\text{ cm}^{-1}$ ,  $1483\text{ cm}^{-1}$ ,  $1520\text{ cm}^{-1}$  and  $1596\text{ cm}^{-1}$ , respectively. We considered that typically 45% of molecules ( $\eta \sim 0.45$ ) were adsorbed on to these Cu NS substrates. The procedure for estimating the enhancement factors (E.F.s) was already reported in our earlier work [11]. The estimated E.F.s for the predominant

mode of  $1342\text{ cm}^{-1}$  were of  $3 \times 10^5$ ,  $2.8 \times 10^5$ ,  $1.9 \times 10^5$ ,  $4.1 \times 10^5$ ,  $1.3 \times 10^5$  and  $2.3 \times 10^5$  for CuS-25, CuS-50, CuS-100, CuS-200, CuS-300 and CuS-400, respectively. The obtained E.F.s was  $\sim 10^5$  for all the 6 type of Cu NSs since they might have produced identical local fields through the excitation of different types of surface plasmons.

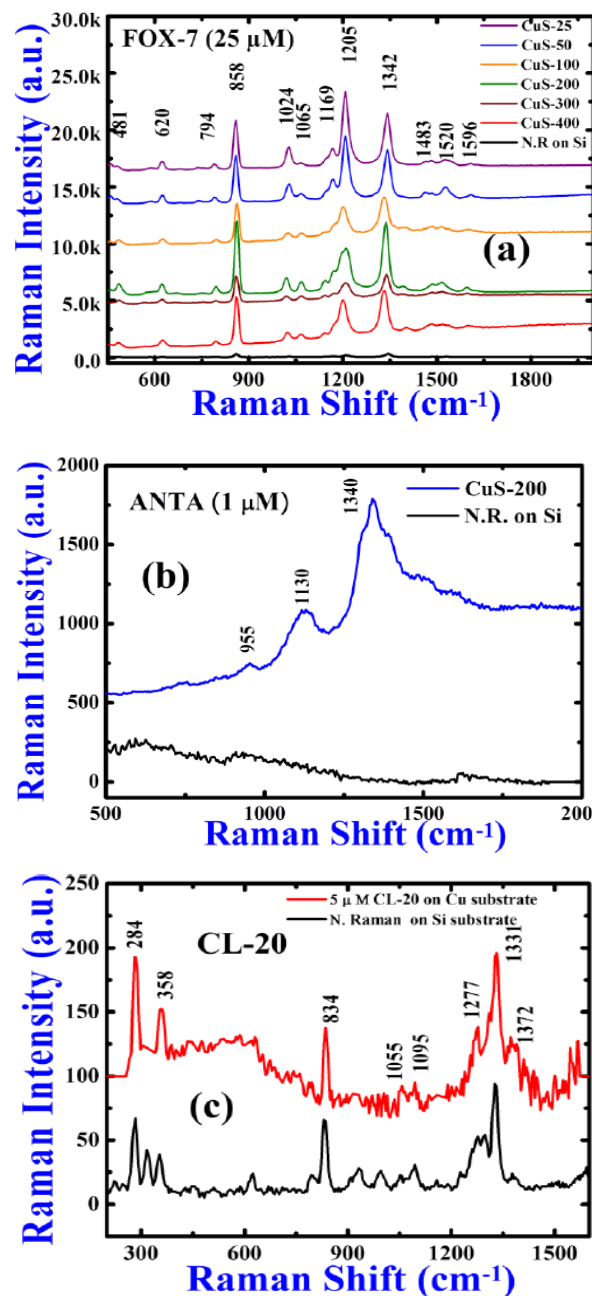


**Fig. 2.** SERS spectra of (a) Fox-7 adsorbed on Cu NSs fabricated through ULAL of Cu in ACN at different pulses energies, (b) ANTA ( $1 \times 10^{-6}$  M) and (c) CL-20 ( $5 \times 10^{-6}$  M) adsorbed on CuS-200. Normal Raman spectrum recorded on silicon substrate is also included in all the figures. The Raman intensity is expressed in arbitrary units (a.u.). N.R. represents normal Raman spectrum.

We had chosen only one SERS active substrate (CuS-200) among the 6 substrates for second measurement of different analyte molecule since all of them demonstrated similar performance in terms of enhancement factors. Secondly, we had chosen ANTA molecule as our second

testing sample to probe the Cu NSs after proper cleaning within a week. **Fig. 2(b)** depicts the SERS spectra of ANTA molecule [**11**] with a concentration of  $1 \times 10^{-6}$  M adsorbed on Cu surface r.m.s. roughness of  $\sim 2.6 \mu\text{m}$  + LIPSS with  $\sim 430$  nm periodicity (CuS-200). The enhancement was notable even at the concentration of  $1 \times 10^{-6}$  M and the Raman peak at  $1340 \text{ cm}^{-1}$ , corresponding to the C-NO<sub>2</sub> symmetric stretch, which is the characteristic peak of ANTA molecule, was elevated. Along with characteristic modes, other modes observed were near  $955 \text{ cm}^{-1}$  and  $1130 \text{ cm}^{-1}$  and those corresponding to N4-C5-N1 bending mode and N-N symmetric stretching mode, respectively. The other Raman modes were not detected at these concentrations which were elevated at higher concentrations (500  $\mu\text{M}$ ) reported in our earlier work [**11**]. It is believed that  $\sim 40\%$  ( $\eta \sim 0.4$ ) molecules were adsorbed on Cu NS substrate. The performance of SERS active substrate has been evaluated by calculating E.F.s. For achieving this, the normal Raman spectrum intensity of ANTA (0.2 M) was compared with enhanced Raman spectrum. The estimated E.F for the characteristic peak of ANTA molecule at  $1340 \text{ cm}^{-1}$  was  $\sim 1.2 \times 10^8$ . The large enhancement in the case of ANTA molecule could be accredited due to huge local field attained through the excitation of strong localized surface plasmons provided by Cu surface with r.m.s. roughness of  $\sim 2.6 \mu\text{m}$ . Furthermore, the substrate could have supported additional field through the propagating surface plasmons due to LIPSS. A week later we chose another explosive molecule (CL-20) with a concentration of  $1 \times 10^{-6}$  M as our third analyte for recording the SERS spectra on the same substrate (CuS-200) following an appropriate cleaning procedure. **Fig. 2(c)** depicts the enhanced Raman spectrum of CL-20 which illustrates the most significant Raman modes [**42**] at  $1331 \text{ cm}^{-1}$  and  $1372 \text{ cm}^{-1}$  corresponding to the characteristic modes (NO<sub>2</sub> symmetric stretch) of the explosive molecule, which are related to nitro-aromatic (or) nitramine group. The other Raman modes significantly enhanced were at  $834 \text{ cm}^{-1}$ ,  $1055 \text{ cm}^{-1}$ ,  $1095 \text{ cm}^{-1}$  and  $1277 \text{ cm}^{-1}$  which correspond to NC torsion + NO<sub>2</sub> deformation, NC torsion + ring torsion + NCH deformation, NN stretch + NC stretch and NO stretch + CC torsion, respectively. It was assumed that  $\sim 40\%$  molecules were adsorbed on the Cu NS substrate. The evaluated E.F. was  $\sim 4.5 \times 10^5$  for the  $1331 \text{ cm}^{-1}$  mode compared with normal Raman spectrum of CL-20 (0.1 M).

#### *Effects of number of pulses on Cu NSs in acetone prepared by $\sim 40$ fs pulses and SERS studies*

**Fig. 3(a-e)** demonstrate the FESEM images of NSs fabricated on the Cu target obtained through fs ablation in acetone with (a)  $N = 253$  (b)  $N = 300$  (c)  $N = 500$  (d)  $N = 1000$  and (e)  $N = 2000$  number of pulses. The scale bar in each of these images is 200 nm. These were achieved at slightly above the threshold fluence of Cu ( $1.7 \pm 0.2 \text{ J/cm}^2$ ) [**40**]. **Fig. 3(a)** illustrates the random nanostructures covering the metal surface and the estimated surface r.m.s. roughness was found to be  $\sim 1.6 \mu\text{m}$  ( $N = 253$  pulses). Following the results from previous reports and our understanding the formation of random nanostructures and

nano-cavities are tentatively ascribed to the hydrodynamical process occurring in the liquid media. With increasing number of laser shots the random nano-roughness turned sharper and heavier. The reason behind the production of heavy and rough NSs could be due to the large absorption by the nanoparticle grains that have been formed by the earlier pulses. The geometrical effects also contribute because of scattering from sharp edges of NSs. After the ablation with  $N=253$  pulses, the threshold fluence of the Cu metal was reduced to  $\sim 0.98 \text{ J/cm}^2$  (before ablation,  $F_{\text{th}} = \sim 2 \text{ J/cm}^2$ ) [**43**].

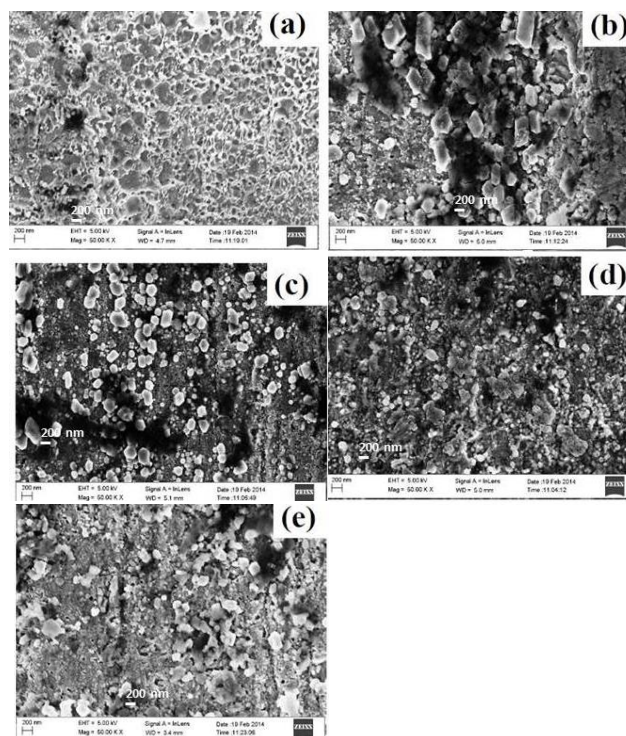


**Fig. 3.** FESEM images of Cu NSs obtained in acetone using fs pulses (a)  $N = 253$ , (b)  $N = 300$ , (c)  $N = 500$ , (d)  $N = 1000$  and (e)  $N = 2000$  pulses. The scale bar is 200 nm in all the pictures.

For the case of ablation with  $N=300$  pulses, cuboids (1  $\sim 400$  nm, b  $\sim 200$  nm, h  $\sim 60$  nm) were produced on the Cu surface and is evident from the data depicted in **Fig. 3(b)**. In this case, the input fluence of the laser pulses ( $\sim 2.5 \text{ J/cm}^2$ ) was more than double the ablation threshold ( $\sim 0.98 \text{ J/cm}^2$ ), and this played a significant role in the growth mechanism. The evolution of NSs in the present case could have taken place due to the existence of unique locations which considerably modify the energy distribution of subsequent interaction of laser shots with the target and generate multiple cavitation bubbles. Depending on the collapse of the bubbles, some of the NPs could form clusters with larger size [**26**, **44**] and these clusters might have been truncated into cuboids or cubes. The ablation threshold reached  $0.95 \text{ J/cm}^2$  after  $N=300$  pulses. The threshold fluence of Cu target was observed to reduce from  $0.95 \text{ J/cm}^2$  to  $0.89 \text{ J/cm}^2$ ,  $0.81 \text{ J/cm}^2$  and  $0.74 \text{ J/cm}^2$  as the pulse number increased from  $N = 300$  to 500, 1000 and 2000 pulses, respectively [**43**]. Following the ablation with  $N = 500$  pulses (**Fig. 3(c)**),  $N=1000$  pulses (**Fig. 3(d)**) and  $N=2000$  pulses (**Fig. 3(e)**),

hexagonal NPs with  $\sim 125$  nm size, spherical NPs with  $\sim 70$  nm and random nano-roughness or nano-cavities with mean size of  $\sim 1.8$   $\mu\text{m}$  were observed, respectively. As observed from the results presented the cuboids were modified into hexagonal structures with reduced size and then finally changed into spherical nanoparticles.

A possible explanation could be the prominence of fragmentation effects with increasing number of input pulses [45]. In each of these cases the surface roughness offered by the targets changed drastically with increasing number of pulses and, consequently, the NSs formed were diverse. Additionally, the production of random nano-cavities could be attributed to the complicated cavitation bubble dynamics in the case of ULAL [26, 44]. The morphology on Cu substrates (after the ablation) could be summarized as (i) random nano-roughness with r.m.s. value of  $\sim 1.6$   $\mu\text{m}$  (ii) cuboid (l  $\sim 400$  nm, b  $\sim 200$  nm, h  $\sim 60$  nm) particles (iii) hexagonal particles with  $\sim 125$  nm size (iv) spherical particles with  $\sim 70$  nm average size and (v) random NSs with r.m.s. roughness of  $\sim 1.8$   $\mu\text{m}$  for a pulse train of  $\sim 253$ ,  $\sim 300$ ,  $\sim 500$ ,  $\sim 1000$  and  $\sim 2000$ , respectively, and they were labeled as CuNS-253, CuNS-300, CuNS-500, CuNS-1000 and CuNS-2000, respectively for clarity. Beyond 2000 pulses, the morphology on the substrates also contained nanostructures, nonetheless, with lower density.

FOX-7 was considered as a probe molecule for recording the SERS spectra. The compound was diluted ( $25$   $\mu\text{M}$ ) and then placed on Cu NSs fabricated using different pulses numbers. A solution with  $0.1$  M concentration was used as reference which was coated on a plain silicon substrate. Subsequently, they were dried and the Raman spectra from nanostructured Cu target and plain Si surfaces were recorded and the obtained data is illustrated in Fig. 4(a). It is evident from the data presented in Fig. 4(a) that the characteristic Raman mode at  $1335$   $\text{cm}^{-1}$  (symmetric C-NO<sub>2</sub> stretching and NH wagging) was observed with lower intensity in the normal Raman spectrum along with some other modes. On the other hand, in SERS spectra the modes were intensified (30-50 times) which were present in normal Raman spectrum with lower intensity. The elevated modes in SERS spectra were the  $483$   $\text{cm}^{-1}$  (symmetric NO and NH wagging),  $620$   $\text{cm}^{-1}$  (out of layer symmetric NH wagging),  $794$   $\text{cm}^{-1}$  (C-NO<sub>2</sub> rocking),  $861$   $\text{cm}^{-1}$  (NO and NH rocking),  $1025$   $\text{cm}^{-1}$  (in-layer asymmetric NH wagging),  $1067$   $\text{cm}^{-1}$  (in-layer symmetric NH wagging),  $1169$   $\text{cm}^{-1}$  (C-C stretch and NH wagging),  $1205$   $\text{cm}^{-1}$  (asymmetric C-NO<sub>2</sub> stretching and NH wagging),  $1483$   $\text{cm}^{-1}$  (Out of layer symmetric NH wagging, NO and NH rocking) and  $1596$   $\text{cm}^{-1}$  (NH<sub>2</sub> bending) modes. To evaluate the performance of these Cu NSs, E.F.'s were estimated by considering the peak intensity in the SERS spectra which was compared with the corresponding peak intensity obtained from the normal Raman spectra. The E.Fs calculated for a particular mode of  $1335$   $\text{cm}^{-1}$  were  $2.0 \times 10^5$ ,  $3.6 \times 10^5$ ,  $7.0 \times 10^5$ ,  $2.8 \times 10^5$  and  $2.3 \times 10^5$  for random NSs with roughness of  $\sim 1.6$   $\mu\text{m}$  (CuNS-250), cuboids with length of  $\sim 400$  nm (CuNS-300), hexagons with  $\sim 90$  nm size (CuNS-500), spherical particles with  $\sim 100$  nm (CuNS-1000) and random NSs with r.m.s. roughness of  $\sim 1.8$   $\mu\text{m}$  (CuNS-2000), respectively. The estimated E.F.s was typically  $10^5$  for all the type of Cu NSs

investigated. However, the substrate with hexagonal NPs demonstrated 2-3 times higher enhancement than substrates containing random NSs, cuboid NPs and spherical NPs. We believe that higher enhancement was obtained due to (a) the intensified local electric field at sharp edges of hexagonal NP which might act as the generators hotspots through the excitation of localized surface plasmons and (b) combined oscillations of surface plasmons due to sharp edges of two hexagonal NPs could have also contributed to the amplification of local field. Fig. 4(b) illustrates the SERS spectra of Rh6G ( $5 \times 10^{-6}$  M) recorded from ablated Cu substrates achieved with different number of pulses after cleaning. Following the procedures listed in earlier reports [6, 11], the observed modes in normal Raman and SERS spectra were assigned.

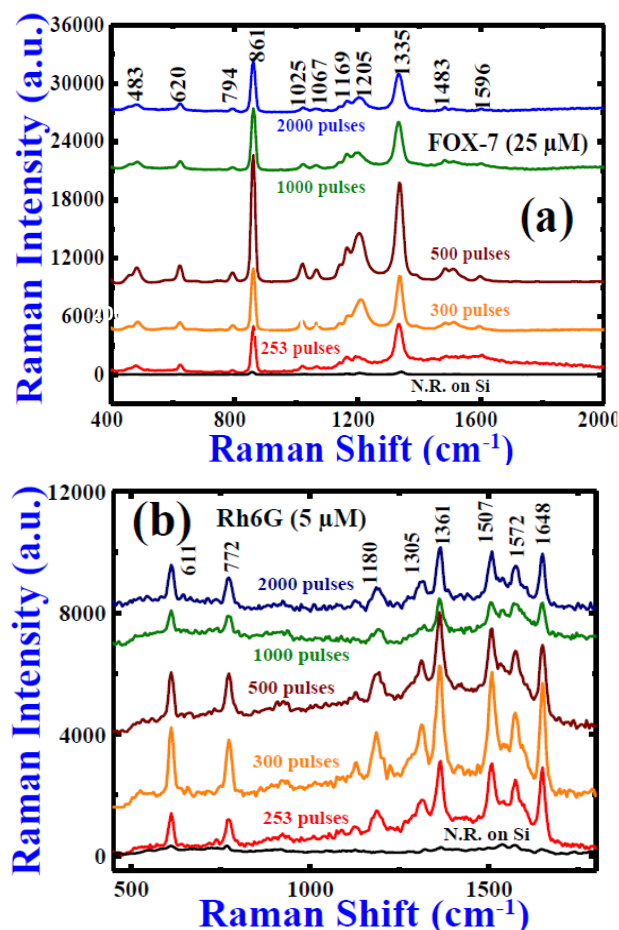


Fig. 4. SERS spectra of (a) FOX-7 ( $25 \times 10^{-6}$  M) and (b) Rh6G ( $5 \times 10^{-6}$  M) adsorbed on Cu NS substrates fabricated through fs ablation in acetone under the influence of pulse number at constant fluence of  $2.5$   $\text{J}/\text{cm}^2$ . The Raman intensity is expressed in arbitrary units (a.u.). N.R. represents normal Raman spectrum.

The Raman mode near  $1361$   $\text{cm}^{-1}$  (corresponding to aromatic C-C stretch vibration) is the characteristic mode of Rh6G molecule. The Raman modes present at  $611$   $\text{cm}^{-1}$ ,  $772$   $\text{cm}^{-1}$  and  $1180$   $\text{cm}^{-1}$  correspond to C-C-C ring in-plane bend, C-H out-of-plane bend, and C-C stretch modes, respectively. The Raman peaks observed at  $1507$   $\text{cm}^{-1}$ ,  $1572$   $\text{cm}^{-1}$  and  $1648$   $\text{cm}^{-1}$  were mainly from the contribution of aromatic C-C stretch. The estimated E.Fs for the principal vibrational mode  $1361$   $\text{cm}^{-1}$  were

$\sim 3.4 \times 10^6$ ,  $\sim 8.4 \times 10^6$ ,  $\sim 6.0 \times 10^6$ ,  $\sim 2.5 \times 10^6$  and  $\sim 3.2 \times 10^6$  for CuNS-250, CuNS-300, CuNS-500, CuNS-1000 and CuNS-2000, respectively. Among all the Cu substrates investigated, CuNS-300 (whose surface morphology comprised cuboids with dimensions of 'l'  $\sim 400$  nm, 'b'  $\sim 200$  nm, 'h'  $\sim 60$  nm), and CuNS-500 (possessing dimers of hexagonal NPs) demonstrated superior enhancement compared to other Cu NSs. Additionally, the reproducibility of SERS measurements was high when the sample was probed at different positions on the SERS active Cu substrate. There are very few reports in literature on the detection of explosives using SERS technique [46-52], in general, and nanostructured substrates/targets, in particular. Hakonen *et al.* [53], very recently, reviewed different SERS substrates and mechanisms used for explosives detection in security applications. They discussed the prospects of SERS becoming an important tool for convenient in-situ threat identification/detection and summarized various existing SERS detection methods and substrates with particular attention on ultra-sensitive real-time detection.

Polavarapu *et al.* [54] discussed the possibilities of low-cost flexible substrates for nanoplasmonic sensing in their review article. Some of the important challenges all the researchers encounter before using the deployment of nanostructured substrates for consistently successful detection of explosives are (a) achieving higher enhancement factors (at least  $10^8$ - $10^{10}$ ) with the intention of detecting pM/fM concentrations effortlessly (b) reliably and reproducibly create large area nanostructures using various techniques involving lower cost and at rapid times [55] (c) identify/understand the mechanism for enhancements for each explosive molecule for a particular morphology of the nanostructured target (d) implement SERS studies with low power laser source and a hand-held Raman spectrometer which can later be integrated to form a compact portable device for on-field detection. Our future studies will focus detecting pM and fM concentration explosive molecules. To achieve this it is imperative to thoroughly understand (a) the ablation mechanisms performed under a variety of conditions [56-58] and (b) the interaction mechanism of the nanostructures with the analyte molecules enabling the preparation of efficient substrates.

## Conclusion

In summary, we have investigated the surface morphologies of Cu NSs such as LIPSS, nano-roughness along with formation of NPs with different shapes in ps laser ablated Cu targets in acetonitrile. The structures were fabricated with varying pulse energies and pulse numbers using ps and fs pulse ablation of Cu in liquid media. In the ps domain the heat diffusion of electrons in the Cu target resulted in the formation of large area LIPSS. The trace level detection of an explosive molecule FOX-7 from Cu NSs, fabricated with different pulse energies, was studied using the SERS technique. Estimated E.F.s for the enhancements for various Raman modes of FOX-7 (25  $\mu$ M) were  $\sim 10^5$  for all the substrates. SERS studies of ANTA and CL-20 molecules were also performed on

recycled CuS-200 target revealing a large enhancement (E.F.s of  $10^5$ - $10^8$ ). Additionally, Cu NS obtained with different pulse numbers in fs domain were also utilized for SERS studies of a FOX-7 molecule along with Rh6G molecule separately after subjecting the substrates to appropriate cleaning procedure and achieved enhancement factors of  $>10^5$ .

## Acknowledgements

Authors acknowledge DRDO, India for continuous financial support and UPE-II, University of Hyderabad for partial financial support.

## Author contributions

Conceived the plan: SVR; Performed the experiments: SH, GKP, AMM; Data analysis: SH, GKP, AMM; Wrote the paper: SH, GKP, SVR. Authors have no competing financial interests.

## Reference

- Nie, S.; Emory, S. R; *Science*, **1997**, 275, 1102.  
DOI: [10.1126/science.275.5303.1102](https://doi.org/10.1126/science.275.5303.1102)
- Moskovits, M; *Rev. Mod. Phys.*, **1985**, 57, 783.  
DOI: [10.1103/RevModPhys.57.783](https://doi.org/10.1103/RevModPhys.57.783)
- Kneipp, K.; Wang, Y.; Kneipp, H.; Perelman, L. T.; Itzkan, I.; Dasari, R. R.; Feld, M.S; *Phys. Rev. Lett.* **1997**, 78, 1667.  
DOI: [10.1103/PhysRevLett.78.1667](https://doi.org/10.1103/PhysRevLett.78.1667)
- Kneipp, K.; Kneipp, H.; Itzkan, I.; Dasari, R. R.; Feld, M.S.; Dresselhaus, M. S; *Top. Appl. Phys.*, **2002**, 82, 227.  
DOI: [10.1007/3-540-44948-5](https://doi.org/10.1007/3-540-44948-5)
- Stiles, P.L.; Dieringer, J. A.; Shah, N. C.; Van Duyne, R.P; *Ann. Rev. Anal. Chem.*, **2008**, 1, 1, 601.  
DOI: [10.1146/annurev.anchem.1.031207.112814](https://doi.org/10.1146/annurev.anchem.1.031207.112814)
- Gopala Krishna, P.; Hamad, S.; Tewari, S. P.; Sreedhar, S.; Prasad, M. D.; Venugopal Rao, S; *J. Appl. Phys.* **2013**, 113, 073106.  
DOI: [10.1063/1.4792483](https://doi.org/10.1063/1.4792483)
- Jiang, X.; Jiang, Z.; Xu, T.; Su, S.; Zhong, Y.; Peng, F.; Su, Y.; He, Y; *Anal. Chem.*, **2013**, 85, 2809.  
DOI: [10.1021/ac303337b](https://doi.org/10.1021/ac303337b)
- Gracie, K.; Correa, E.; Mabbott, S.; Dougan, J. A.; Graham, D.; Goodacre, R.; Faulds, K; *Chem. Sci.*, **2014**, 5, 1030.  
DOI: [10.1039/C3SC52875H](https://doi.org/10.1039/C3SC52875H)
- Botti, S.; Almaviva, S.; Cantarini, L.; Palucci, A.; Puiu, A.; Rufolon, A; *J. Raman Spectrosc.*, **2013**, 44, 463.  
DOI: [10.1002/jrs.4203](https://doi.org/10.1002/jrs.4203)
- Guerrini, L.; Graham, D; *Chem. Soc. Rev.*, **2012**, 41, 7085.  
DOI: [10.1039/C2CS35118H](https://doi.org/10.1039/C2CS35118H)
- Hamad, S.; Gopala Krishna, P.; Ahamad Mohiddon, M.; Venugopal Rao, S; *Appl. Phys. Lett.* **2014**, 104, 263104.  
DOI: [10.1063/1.4885763](https://doi.org/10.1063/1.4885763)
- Gopala Krishna, P.; Hamad, S.; Ahamad Mohiddon, M.; Venugopal Rao, S; *Appl. Surf. Sci.*, **2014**, 303, 217.  
DOI: [10.1016/j.apsusc.2014.02.152](https://doi.org/10.1016/j.apsusc.2014.02.152)
- Hamad, S.; Gopala Krishna, P.; Ahamad Mohiddon, M.; Venugopal Rao, S; *Chem. Phys. Lett.*, **2015**, 621, 171.  
DOI: [10.1016/j.cplett.2015.01.006](https://doi.org/10.1016/j.cplett.2015.01.006)
- Willets, K.A.; and Van Duyne, R.P; *Ann. Rev. Phys. Chem.*, **2007**, 58, 267.  
DOI: [10.1146/annurev.physchem.58.032806.104607](https://doi.org/10.1146/annurev.physchem.58.032806.104607)
- Mishra, Y. K.; Mohapatra, S.; Singhal, R.; Avasthi, D. K.; Agarwal, D. C.; Ogale, S. C; *Appl. Phys. Lett.*, **2008**, 92, 043107.  
DOI: [10.1063/1.2838302](https://doi.org/10.1063/1.2838302)
- Mohapatra, S.; Mishra, Y. K.; Warriar, A. M.; Philip, R.; Sahoo, S.; Arora, A.K.; Avasthi, D.K; *Plasmonics*, **2012**, 7, 25.  
DOI: [10.1007/s11468-011-9271-y](https://doi.org/10.1007/s11468-011-9271-y)
- Mishra, Y.K.; Adelung, R.; Kumar, G.; Elbahri, M.; Mohapatra, S.; Singhal, R.; Tripathi, A.; Avasthi, D.K; *Plasmonics* **2013**, 8, 811.  
DOI: [10.1007/s11468-013-9477-2](https://doi.org/10.1007/s11468-013-9477-2)
- Fontana, J.; Livenere, J.; Bezares, F. J.; Caldwell, J. D.; Rendell, R.; Ratna, B. R; *Appl. Phys. Lett.*, **2013**, 102, 201606.  
DOI: [10.1063/1.4807659](https://doi.org/10.1063/1.4807659)
- Gopala Krishna, P.; Hamad, S.; Ahamad Mohiddon, M.; Venugopal Rao, S; *Laser Phys. Lett.*, **2015**, 12, 036003.  
DOI: [10.1088/1612-2011/12/3/036003](https://doi.org/10.1088/1612-2011/12/3/036003)

20. Vendamani, V.S.; Hamad, S.; Saikiran, S.; Nageswara Rao, S.V.S.; Venugopal Rao, S.; Pathak, A.P.; *J. Mater. Sci.* **2015**, *50*, 1666.  
DOI: [10.1007/s10853-014-8727-9](https://doi.org/10.1007/s10853-014-8727-9)
21. Venugopal Rao, S.; Gopala Krishna, P.; Hamad, S.; *J. Nanosci. Nanotech.* **2014**, *14*, 1364.  
DOI: [10.1166/jnn.2014.9138](https://doi.org/10.1166/jnn.2014.9138)
22. Itina, T.; *J. Phys. Chem. C*, **2011**, *115*, 5044.  
DOI: [10.1021/jp1090944](https://doi.org/10.1021/jp1090944)
23. Yang, G. W.; Jin-Bin, W.; Qui-Xiang, L.; *J. Phys.: Condens. Matter* **1998**, *10*, 7923.  
DOI: [10.1088/0953-8984/10/35/024](https://doi.org/10.1088/0953-8984/10/35/024)
24. Yang, G. W.; *Prog. Mater. Sci.*, **2007**, *52*, 648.  
DOI: [10.1016/j.pmatsci.2006.10.016](https://doi.org/10.1016/j.pmatsci.2006.10.016)
25. Liu, P.; Cui, H.; Wang, C. X.; Yang, G. W.; *Phys. Chem. Phys. Chem.*, **2010**, *12*, 3942.  
DOI: [10.1039/b918759f](https://doi.org/10.1039/b918759f)
26. Yang, Y.; Yang, J.; Liang, C.; Wang, H.; Zhu, X.; Zhang, N.; *Opt. Exp.* **2009**, *17*, 21124.  
DOI: [10.1364/OE.17.021124](https://doi.org/10.1364/OE.17.021124)
27. Miyaji, G.; Miyazaki, K.; *Opt. Exp.* **2008**, *16*, 16265.  
DOI: [10.1364/OE.16.016265](https://doi.org/10.1364/OE.16.016265)
28. Hopp, B.; Smausz, T.; Csizmadia, T.; Vass, C.; Tápai, C.; Kiss, B.; Ehrhardt, M.; Lorenz, P.; Zimmer, K.; *Appl. Phys. A* **2013**, *113*, 291.  
DOI: [10.1007/s00339-013-7913-y](https://doi.org/10.1007/s00339-013-7913-y)
29. Bashir, S.; Rafique, M. S.; Nathala, C. S.; Husinsky, W.; *Appl. Surf. Sci.* **2014**, *290*, 53.  
DOI: [10.1016/j.apsusc.2013.10.187](https://doi.org/10.1016/j.apsusc.2013.10.187)
30. Vorobyev, A. Y.; Makin, V. S.; Guo, C.; *J. Appl. Phys.* **2007**, *101*, 034903.  
DOI: [10.1063/1.2432288](https://doi.org/10.1063/1.2432288)
31. Gopala Krishna, P.; Hamad, S.; Sreedhar, S.; Tewari, S. P.; Venugopal Rao, S.; *Chem. Phys. Lett.* **2012**, *530*, 93.  
DOI: [10.1016/j.cplett.2012.01.081](https://doi.org/10.1016/j.cplett.2012.01.081)
32. Tanvir Ahmmed, K. M.; Grambow, C.; Anne-Marie, K.; *Micromachines* **2014**, *5*, 1219.  
DOI: [10.3390/mi5041219](https://doi.org/10.3390/mi5041219)
33. Skolski, J. Z. P.; Römer, G. R. B. E.; Vincenc Obona, J.; Huisin't Veld, A. J.; *J. Appl. Phys.* **2014**, *115*, 103102.
34. Huang, M.; Zhao, F.; Cheng, Y.; Xu, N.; Xu, Z.; *Phys. Rev. B* **2009**, *79*, 125436.  
DOI: [10.1103/PhysRevB.79.125436](https://doi.org/10.1103/PhysRevB.79.125436)
35. Derrien, T. J. Y.; Itina, T. E.; Torres, R.; Sarnet, T.; Sentis, M.; *J. Appl. Phys.*, **2013**, *114*, 083104.  
DOI: [10.1063/1.4818433?ver=pdfcov](https://doi.org/10.1063/1.4818433?ver=pdfcov)
36. Hamad, S.; Gopala Krishna, P.; Vendamani, V. S.; Nageswara Rao, S.V.S.; Pathak, A. P.; Tewari, S. P.; Venugopal Rao, S.; *J. Phys. Chem. C* **2014**, *118*, 7139.  
DOI: [10.1021/jp501152x](https://doi.org/10.1021/jp501152x)
37. Wang, J.; Guo, C.; *J. Appl. Phys.*, **2006**, *100*, 023511.  
DOI: [10.1063/1.2214464](https://doi.org/10.1063/1.2214464)
38. Hamad, S.; Gopala Krishna, P.; Tewari, S. P.; Venugopal Rao, S.; *J. Phys. D: Appl. Phys.* **2013**, *46*, 485501.  
DOI: [10.1088/0022-3727/46/48/485501](https://doi.org/10.1088/0022-3727/46/48/485501)
39. Gopala Krishna, P.; Hamad, S.; Venugopal Rao, S.; *J. Phys. Chem. C*, **2015**, *119*, 16972.  
DOI: [10.1021/acs.jpcc.5b03958](https://doi.org/10.1021/acs.jpcc.5b03958)
40. Huynh, T. T. D.; Semmar, N.; *Appl. Phys. A*, **2014**, *116*.  
DOI: [10.1007/s00339-014-8255-0](https://doi.org/10.1007/s00339-014-8255-0)
41. Barcikowski, S.; Menéndez-Manjón, A.; Chichkov, B.; Brikas, M.; Gediminas, R.; *Appl. Phys. Lett.* **2007**, *91*, 083113.  
DOI: [10.1063/1.2773937](https://doi.org/10.1063/1.2773937)
42. Ghosh, M.; Venkatesan, V.; Sikder, N.; Sikder, A. K.; *Central Euro. J. Energetic Mater.* **2013**, *10*, 419.
43. Liang, F.; Vall'ee, R.; Gingras, D.; Leang Chin, S.; *Opt. Mat. Exp.* **2011**, *1*, 1244.  
DOI: [10.1364/OME.1.001244](https://doi.org/10.1364/OME.1.001244)
44. Vogel, A.; Linz, N.; Freidank, S.; Paltauf, G.; *Phys. Rev. Lett.* **2008**, *100*, 038102.  
DOI: [10.1103/PhysRevLett.100.038102](https://doi.org/10.1103/PhysRevLett.100.038102)
45. Lorazo, P.; Lewis, P. J.; Meunier, M.; *Phys. Rev. Lett.* **2003**, *91*, 225502.  
DOI: [10.1103/PhysRevLett.91.225502](https://doi.org/10.1103/PhysRevLett.91.225502)
46. Farrell, M.E.; Holthoff, E.L.; Pellegrino, P.M.; *Appl. Spectrosc.* **2014**, *68*, 287.  
DOI: [10.1366/13-07035](https://doi.org/10.1366/13-07035)
47. Wackerbarth, H.; Gundrum, L.; Salb, C.; Christou, K.; Viöl, W.; *Appl. Opt.* **2010**, *49*, 4367.  
DOI: [10.1364/AO.49.004367](https://doi.org/10.1364/AO.49.004367)
48. Wackerbarth, H.; Salb, C.; Gundrum, L.; Niederkrüger, M.; Christou, K.; Beushausen, V.; Viöl, W.; *Appl. Opt.* **2010**, *49*, 4362.  
DOI: [10.1364/AO.49.004362](https://doi.org/10.1364/AO.49.004362)
49. Botti, S.; Cantarini, L.; Palucci, A.; *J. Raman. Spectrosc.* **2010**, *41*, 866.  
DOI: [10.1002/jrs.2649](https://doi.org/10.1002/jrs.2649)
50. Wang, X.; Shi, W.; She, G.; Mu, L.; *Phys. Chem. Chem. Phys.* **2012**, *14*, 5891.  
DOI: [10.1039/c2cp40080d](https://doi.org/10.1039/c2cp40080d)
51. Sajanlal, P. R.; Pradeep, T.; *Nanoscale* **2012**, *4*, 3427.  
DOI: [10.1039/c2nr30557g](https://doi.org/10.1039/c2nr30557g)
52. Baker, G.A.; Moore, D.S.; *Anal. Bioanal. Chem.* **2005**, *382*, 1751.  
DOI: [10.1007/s00216-005-3353-7](https://doi.org/10.1007/s00216-005-3353-7)
53. Hakonen, A.; Andersson, P. O.; Schmidt, M. S.; Rindzevicius T.; Käll, M.; *Analytica Chimica Acta*, **2015**, *893*, 1.  
DOI: [10.1016/j.aca.2015.04.010.s](https://doi.org/10.1016/j.aca.2015.04.010.s)
54. Polavarapu, L.; Liz-Marzán, L. M.; *Phys. Chem. Chem. Phys.* **2013**, *15*, 5288.  
DOI: [10.1039/C2CP43642F](https://doi.org/10.1039/C2CP43642F)
55. Zheng, G.; Polavarapu, L.; Liz-Marzán, L.M.; Pastoriza-Santos, I.; Pérez-Juste, J.; *Chem. Commun.* **2015**, *51*, 4572.  
DOI: [10.1039/c4cc09466b](https://doi.org/10.1039/c4cc09466b)
56. Noël, S.; Hermann, J.; Itina, T.E.; *Appl. Surf. Sci.* **2007**, *253*, 6310.  
DOI: [10.1016/j.apsusc.2007.01.081](https://doi.org/10.1016/j.apsusc.2007.01.081)
57. Hermann, J.; Noël, S.; Itina, T.E.; Axente, E.; Povarnitsyn, M. E.; *Las. Phys.* **2008**, *18*, 374.  
DOI: [10.1134/s11490-008-4002-6](https://doi.org/10.1134/s11490-008-4002-6)
58. Povarnitsyn, M.E.; Itina, T.E.; *Appl. Phys. A* **2014**, *117*, 175.  
DOI: [10.1007/s00339-014-8319-1](https://doi.org/10.1007/s00339-014-8319-1)

## Advanced Materials Letters

Copyright © VBRI Press AB, Sweden  
[www.vbripress.com](http://www.vbripress.com)

Publish your article in this journal

Advanced Materials Letters is an official international journal of International Association of Advanced Materials (IAAM, [www.iaamonline.org](http://www.iaamonline.org)) published by VBRI Press AB, Sweden monthly. The journal is intended to provide top-quality peer-review articles in the fascinating field of materials science and technology particularly in the area of structure, synthesis and processing, characterisation, advanced-state properties, and application of materials. All published articles are indexed in various databases and are available download for free. The manuscript management system is completely electronic and has fast and fair peer-review process. The journal includes review article, research article, notes, letter to editor and short communications.

